Pergamon

Int. J. Solids Structures Vol. 31, No. 7, pp. 985–1002, 1994

0020-7683/94 $6.00 + .00

FRACTURE ALONG AN INTERLAYER

WEI YANG
Department of Engineering Mechanics, Tsinghua University, Beijing 100084, China

and

C. FONG SHIH
Division of Engineering, Brown University, Providence, RI 02912, U.S.A.

(*Received* 7 *February* 1993)

Abstract—A nonhomogeneous interlayer is introduced between two dissimilar materials to characterize the transition of the elastic moduli across the bimaterial interface. The $1/\sqrt{r}$ singularity field near the tip of an advancing interlayer crack is related to the remote interface crack tip field for general aligned orthotropic bimaterials. An approximate but explicit relation for the phase shift between the near tip and the remote singularity fields is derived. Comparisons with analytical and numerical solutions show that the relation is fairly accurate. The interlayer model provides insightful interpretations of several important concepts of interface fracture mechanics, such as stress oscillation, near tip contact and mode mixity. For crack tip mode mixity, ψ^{tip}, in the range $-\pi/2 < \psi^{\text{tip}} < \pi/2$, the crack tip is truly open. The crack is partially closed for $\psi^{\text{tip}} = \pm\pi/2$. Plasticity effects associated with dislocation emissions from the crack tip are also considered.

1. INTRODUCTION

An account of a pragmatic engineering methodology which allows the fracture resistance of interfaces to be measured and utilized is documented in an Acta-Scripta Metallurgica Proceedings (1990) and a comprehensive article by Hutchinson and Suo (1992). The rapid progress that was made in the late 1980s on this subject can be attributed to two concepts: (i) small scale contact zone and (ii) mode mixity. The concept of a small scale contact zone circumvents the pathological aspects of the oscillatory singularity and permits the argument to be made that the complex stress intensity factor is the appropriate crack tip characterizing parameter (Rice, 1988).

Mode mixity is an important feature of interface fracture (Rice, 1988; Shih and Asaro, 1988; Hutchinson, 1990). Because of the oscillatory singularity the relative proportion of (in-plane) shear to normal tractions on the bonding plane, i.e. the mode mixity, varies with distance ahead of the crack tip. Mode mixity can be unambiguously defined by the ratio of the shear to normal tractions at a distance $\hat{L}$ ahead of the crack (Rice, 1988). Though the choice of $\hat{L}$ is arbitrary, a fixed value of $\hat{L}$ for the material pair provides a common measure of mode mixity and allows the interface toughness data from different crack geometries to be organized into a single curve of toughness vs mode mixity. The interface fracture toughness curve, a property of the material pair, is a key element of a pragmatic engineering methodology. These aspects are elaborated upon by Hutchinson and Suo (1992), Shih (1991) and O'Dowd *et al.* (1992).

There are advantages to assigning a microstructural identity to $\hat{L}$, namely an interlayer zone thickness. The interlayer zone, which can be the reaction layer or the interdiffusion zone, need not be precisely established since a thickness dimension broadly representative of the interface structure is all that is required. However once a choice is made for the material pair, it must be used consistently. Several attractive features emerge with this approach leading to clarification of certain concepts. For example the crack tip field is nonoscillatory so that the local mode mixity does not vary with distance ahead of the crack tip. The local stress modes are defined by the conventional K_{I} and K_{II} stress intensity factors. These are related to the remote complex stress intensity factor by a relation which depends on the interlayer thickness and the elastic properties of the interlayer and the material pair. Stress oscillation may not be an issue at all and related problems of an "open crack" and small scale contact can be dealt with directly.

The interlayer mentioned above is a transition layer where the elastic moduli vary continuously between those of the two materials as discussed by Delale and Erdogan (1988). The thickness of this transition layer, hereafter denoted by $2h$, ranges from nanometers for an atomistically sharp interface (e.g. Ruhle *et al.*, 1990; O'Dowd *et al.*, 1992) to fractions of a millimeter for a fully diffused bimaterial interface. The interlayer thickness and elastic modulus can be estimated by one of several methods: the unloading portion of the indentation curve produced by a nanoindentor (Nix, 1989), line scans on various material phases by electron optical methods (Whan, 1986) and high resolution scanning acoustic microscope (Ahn *et al.*, 1991). Investigators are also exploring various processing techniques to tailor the composition gradient and microstructure variation with the aim of producing a gradual variation of mechanical properties between two distinctly dissimilar substrates.

These developments provide the impetus for considering an interlayer model with moduli varying across the finite width as depicted in Fig. 1. The semi-infinite crack lies on the x_1 axis and advances in a straight or zigzag manner within the interlayer. The elasticity tensor varies smoothly and monotonically from the upper material moduli C^+_{ijkl} at $x_2 = h$ to the lower material moduli C^-_{ijkl} at $x_2 = -h$ via an arbitrarily prescribed material transition function (defined in Section 3). However the elasticity tensor does not vary in the x_1 direction. The model introduces another length to the present framework of interface fracture while its mathematical tractability brings about a greater clarity of interlayer fracture than is possible with the model used by Delale and Erdogan (1988). The concept of interlayer fracture is pertinent to either a diffuse interface or a wavy (or zigzag) interface, as illustrated in Figs 2(a, b), respectively.

The general structure of the crack tip solution within the interlayer is constructed and then connected to the remote K^∞ field for an aligned orthotropic bimaterial by appealing to the J integral. Only one real material related parameter, namely the phase shift angle ω, is left unspecified. The values of ω are estimated in Section 3 by the auxiliary functions ω_+ and ω_- which are related to the phase shift angle ϕ (Hutchinson *et al.* 1987) for a crack paralleling an interface between dissimilar materials, attributed to the material mismatch. The auxiliary functions are used to construct a multi-ply bimaterial model to estimate ω values for monotonic material transition functions. The accuracy of the procedure is confirmed by comparing the estimated phase shift with the analytical solutions of Delale and Erdogan (1988) and recent finite element calculations.

Related issues of stress oscillation and crack tip contact are dealt with directly. The crack tip is truly open (free of any form of contact) for $-\pi/2 < \psi^{tip} < \pi/2$. For partially

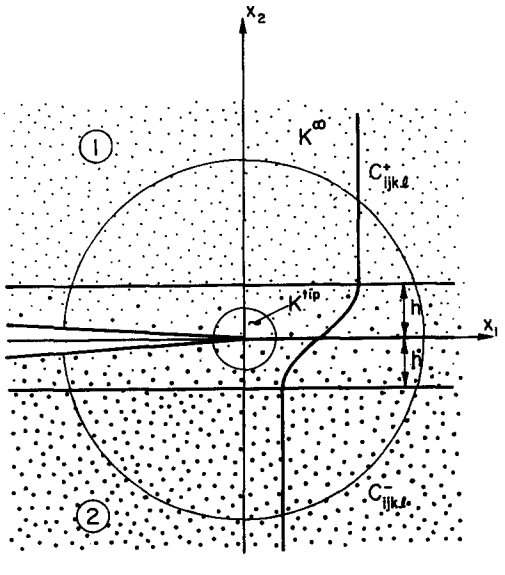

(b)

Fig. 1. A mechanics model for interlayer fracture.

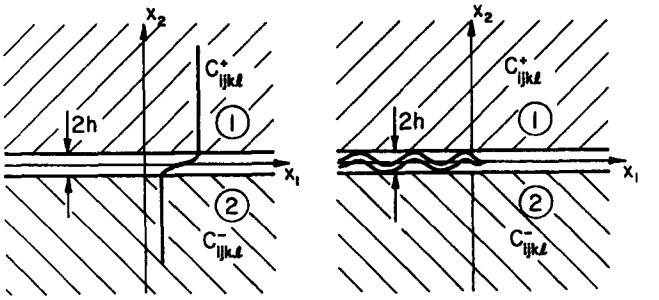

Fig. 2. Various types of interlayers, (a) a transition layer between bimaterials, (b) a wavy (or rough) interface.

closed cracks, $\psi^{tip} = \pm\pi/2$, we introduce the concept of small scale interlayer contact. The interlayer fracture model effectively removes the singularity of normal contact stress near the crack tip, as would be predicted by the Comninou model (Comninou, 1977). The fracture behavior of a partially closed interface crack appears to be controlled by the competition between near-tip shearing and remote tensile cracking. The conditions for emission of dislocations from the crack tip and the effect of near tip mode mixity on dislocation emission angles are discussed.

2. GENERAL STRUCTURE OF CRACK TIP SOLUTION

Attention is now focused on the mechanics analysis of the interlayer fracture model depicted in Fig. 1, where the materials above and beneath the interlayer, as well as the nonhomogeneous material within it are restricted to be orthotropic with principal axes aligned with the interfaces (the crack front is normal to the principal plane). The physical length of the interface crack, designated by L, is assumed to be several orders of magnitude larger than the interlayer width $2h$. Along the crack extension line, the bimaterial interface field dominates at a distance $x_1 \gg h$ (equivalently the interlayer can be thought of as shrunk to a mathematically sharp interface). The generalized traction t along x_1 axis in the region far ahead of the crack tip has the form:

$$t(x_1) \equiv \sigma_{22} + i\eta^{\infty}\sigma_{21} = \frac{K^{\infty}}{\sqrt{2\pi x_1}} x_1^{i\varepsilon} \quad x_1 \gg h. \tag{1}$$

The above relation defines a remote complex stress intensity factor K^{∞} for anisotropic bimaterials consistent with the definition proposed by Hutchinson *et al.* (1987), and by Rice (1988) for the special case of isotropic bimaterials. η^{∞} in (1) represents the traction resolution factor for anisotropic materials and provides a unified representation of mode mixity (Wang *et al.*, 1992; Yang *et al.*, 1991). The superscript ∞ and the superscript tip (to be employed shortly) designate quantities associated with the remote and near tip fields, respectively. Since $x_1^{i\varepsilon} = \exp(i\varepsilon \ln x_1) = \cos(\varepsilon \ln x_1) + i \sin(\varepsilon \ln x_1)$, the traction components rotate as x_1 varies. Be that as it may, the stress oscillation near the crack tip may never take place because relation (1) only applies at $x_1 \gg h$.

For aligned orthotropic bimaterials, the traction resolution factor η is given by:

$$\eta = \sqrt{H_{11}/H_{22}}, \tag{2}$$

where the H's are the elements of the bimaterial Hermitian matrix. Explicit expression for H for aligned orthotropic bimaterials is well-documented in the literatures, e.g. Suo (1990), Wang *et al.* (1992). For the in-plane problems, these coefficients are:

$$H_{11}^{\infty} = [2n\lambda^{1/4}\sqrt{s_{11}s_{22}}]^{+} + [2n\lambda^{1/4}\sqrt{s_{11}s_{22}}]^{-}$$
$$H_{22}^{\infty} = [2n\lambda^{-1/4}\sqrt{s_{11}s_{22}}]^{+} + [2n\lambda^{-1/4}\sqrt{s_{11}s_{22}}]^{-}$$
$$H_{12}^{\infty} = i[\sqrt{s_{11}s_{22}}+s_{12}]^{+} - i[\sqrt{s_{11}s_{22}}+s_{12}]^{-}. \tag{3}$$

Here $[\ ]^{+}$ designate quantities for the upper material, and $[\ ]^{-}$ for the lower material. The conventional notation of six by six compliance matrix $\{s_{ij}\}$ is adopted, and the elements are related to the Young's moduli, shear modulus and Poisson's ratios, e.g., $s_{11} = 1/E_1$, $s_{22} = 1/E_2$, $s_{66} = 1/G_{12}$ and $s_{12} = -\nu_{12}/E_1 = -\nu_{21}/E_2$. λ and n in (3) are defined by:

$$\lambda = \frac{s_{11}}{s_{22}}, \quad n = \sqrt{\frac{1}{2} + \frac{2s_{12}+s_{66}}{4(s_{11}s_{22})^{1/2}}}. \tag{4}$$

They measure the in-plane orthotropy: $\lambda = n = 1$ for isotropic solids and $\lambda = 1$ for solids with cubic symmetry. Ellipticity implies that both λ and n should be positive. The definitions (3) and (4) pertain to plane stress, but are also valid for plane strain if s_{ij} is replaced by $s'_{ij} = s_{ij} - s_{i3}s_{j3}/s_{33}$.

The generalized Dundurs' parameters α and β are given by:

$$\alpha = \frac{[\sqrt{s_{11}s_{22}}]^{-} - [\sqrt{s_{11}s_{22}}]^{+}}{[\sqrt{s_{11}s_{22}}]^{-} + [\sqrt{s_{11}s_{22}}]^{+}}, \quad \beta = \frac{iH_{12}^{\infty}}{(H_{11}^{\infty}H_{22}^{\infty})^{1/2}}, \tag{5}$$

the latter is related to the oscillation index ε in (1) by:

$$\varepsilon = \frac{1}{2\pi} \ln \frac{1-\beta}{1+\beta}. \tag{6}$$

The energy release rate $\mathcal{G}^{\infty}$, as determined by the J integral evaluated along a remote contour, is given by:

$$\mathcal{G}^{\infty} = \frac{H_{22}^{\infty}}{4\cosh^2 \pi\varepsilon} |K^{\infty}|^2. \tag{7}$$

Now direct attention to distances $|x_1| \ll h$. The near tip field is governed by the classical $1/\sqrt{r}$ singularity field referred to the material property in the proximity of crack tip provided that continuum analysis still furnishes a valid approximation to the near tip field. The generalized traction along the crack extension line has the following form:

$$t(x_1) \equiv \sigma_{22} + i\eta^{\text{tip}}\sigma_{21} = \frac{K^{\text{tip}}}{\sqrt{2\pi x_1}} \quad x_1 \ll h. \tag{8}$$

Observe that both K^{∞} and K^{tip} do not reduce to the classical definition of complex stress intensity factor $K_{\text{I}} + iK_{\text{II}}$ when $\varepsilon = 0$, unless the traction resolution factor η defined in (2) equals unity. We can conclude from (8) that stress oscillation does not occur as long as the first contact distance r_c, predicted by the field based on the mathematically sharp interface, is comparable to some fraction of the interlayer thickness h. If r_c is estimated using the remote field (1) (Rice, 1988), the nonpathological condition can be phrased as:

$$c_{\text{oscil}} \frac{h}{L} > \exp[-(\pi/2 + \psi^{\infty})/\varepsilon], \tag{9}$$

where the dimensionless number c_{oscil} is a fraction of unity, say about one half, and ψ^{∞} is the mode mixity of (remote) load defined by:

$$\psi^{\infty} \equiv \arctan \frac{\eta^{\infty}\sigma_{21}^{\infty}}{\sigma_{22}^{\infty}}, \tag{10}$$

which does not depend on any length parameters. The energy release rate, $\mathcal{G}^{\text{tip}}$, as evaluated by J integral along a contour shrunk onto the crack tip, is given by:

$$\mathcal{G}^{\text{tip}} = \tfrac{1}{4} H_{22}^{\text{tip}} |K^{\text{tip}}|^2, \quad H_{22}^{\text{tip}} = 4[n\lambda^{-1/4}\sqrt{s_{11}s_{22}}]^{\text{tip}} \tag{11}$$

where n and λ are evaluated using (4) with s_{ij} appropriate to the (crack tip) local material compliances.

The material in Fig. 1 is homogeneous along x_1 direction. This allows us to make use of the path independent J integral to get

$$|K^{\text{tip}}| = q|K^{\infty}|, \tag{12}$$

where the possibility of a contact zone near the crack tip is neglected for the moment. Relative to remote applied K^{∞}, the near tip stress intensity is scaled by a positive and real transmission factor q given by:

$$q = \frac{\sqrt{H_{22}^{\infty}/H_{22}^{\text{tip}}}}{\cosh \pi\varepsilon}, \tag{13}$$

which involves the material properties pertaining to the near tip (homogeneous) region and the remote bimaterial. The q here follows the notation used by Hutchinson *et al.* (1987) for crack paralleling an isotropic bimaterial interface.

By dimensional analysis, the near tip complex stress intensity factors should scale as a linear combination of $K^{\infty}h^{i\varepsilon}$ and its complex conjugate weighted individually by some dimensionless complex numbers. Restricting the result in (12) to the range of admissible mode mixities we obtain:

$$K^{\text{tip}} = q\, e^{i\omega} K^{\infty} h^{i\varepsilon}, \tag{14}$$

by mathematical arguments similar to those employed by Hutchinson *et al.* (1987), and Suo and Hutchinson (1989) for isotropic bimaterials. The real-valued quantity ω depends only on the elastic moduli and therefore represents the material related phase shift from the remote field to the near tip field. It is the only parameter not determined by an application of the J integral. We should point out that the adoption of the traction resolution factor η, as incorporated in the definitions of stress intensity factors in (1) and (8), enables us to derive the general structure connecting K^{∞} to K^{tip} as shown in (14) for aligned orthotropic materials. For the special case of isotropic bimaterials, we have:

$$\eta^{\infty} = \eta^{\text{tip}} = 1, \quad q = \frac{\sqrt{E^{\text{tip}}/E^{\infty}}}{\cosh \pi\varepsilon}, \tag{15}$$

where E^{∞} and E^{tip} are the plane strain tensile moduli for bimaterial and near-tip material, respectively and:

$$\frac{2}{E^{\infty}} = \frac{1-\nu_+^2}{E_+} + \frac{1-\nu_-^2}{E_-}, \quad E^{\text{tip}} = \left[\frac{E}{1-\nu^2}\right]^{\text{tip}}. \tag{16}$$

Though not explicitly noted by Delale and Erdogan (1988), their crack tip stress intensity factor data also shows that the phase shift is independent of the remote loading mode when the crack size is much larger than the interlayer width.

3. ESTIMATE OF PHASE SHIFT

The near tip field within the interlayer, apart from a shift angle ω, is constructed in the preceding section. A method to estimate the phase shift is now detailed. Estimate of ω can be facilitated by using the auxiliary functions ω_+ and ω_- representing phase shift angles for the special cases depicted in Figs 3(a, b). The same geometries are also viewed from the x_1 direction in Fig. 4(a) and outlined by the dashed lines marked by ω_+ and ω_-, respectively. We observe, for the particular case of isotropic bimaterials, that the auxiliary functions ω_- are identical to the angles $\phi(\alpha, \beta)$ tabulated in the paper by Hutchinson *et al.* (1987) for crack paralleling an interface between dissimilar materials. These values, calculated by an integral equation technique, are accurate to within "a small fraction of a percent".

The other auxiliary function ω_+ for the phase shift angle can be obtained by simply switching the upper and lower material assignment, and a change of the sense of the coordinate directions. Taking note of the formulae in (5) and (3), we arrive at:

$$\omega_+(\alpha, \beta) = -\omega_-(-\alpha, -\beta). \tag{17}$$

For realistic values of α and β, an inspection of the data listed in Table 1 of Hutchinson *et al.* (1987) indicates that the value of $\omega_-(\alpha, \beta)$ is small and is nearly equal to $-\omega_-(-\alpha, -\beta)$. Hutchinson *et al.* (1987) have proposed, for sufficiently small α and β, an approximate formula for ω_- which is the first equality given below:

$$\omega_- \approx 0.1584\alpha + 0.0630\beta \approx \omega_+. \tag{18}$$

The linear dependence of ω_- on α and β shown by first equality in (18) and the mirror symmetry behavior of ω_+ and ω_- as indicated in (17) implies the second relation in (18).

An estimate of ω for a general interlayer model can be obtained by using the multi-ply model as shown in Fig. 4(a). A bimaterial cross-section of unit thickness containing the interlayer is assumed to be represented by many bimaterial thin plies. The division line of material C^+_{ijkl} and material C^-_{ijkl} is denoted by the solid stair-step curve which approaches the smooth dot-dashed line when the ply thickness is taken to be infinitesimal. Accordingly, the thickness averaged elastic moduli at the location $x_2 = yh$ is given by the mixture rule:

$$C_{ijkl}(y) = [1 - z(y)]C^+_{ijkl} + z(y)C^-_{ijkl} \tag{19}$$

where $z(y)$, as referred to the coordinate system set up in Fig. 4(a), characterizes the dot-dashed bounding curve in Fig. 4(a). Both z and y are dimensionless, and the sequence of thin plies can be shuffled around as long as their thickness composition obeys the same $z(y)$ function, termed as the material transition function in the sense of (19). This transition

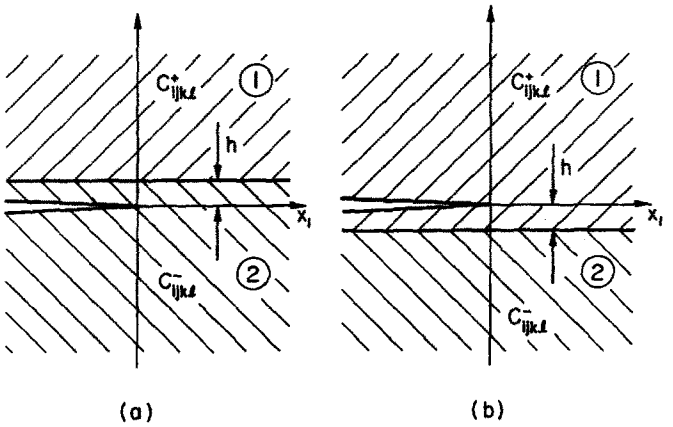

Fig. 3. Bounds of phase shifting angle, (a) limiting case ω_-, (b) limiting case ω_+.

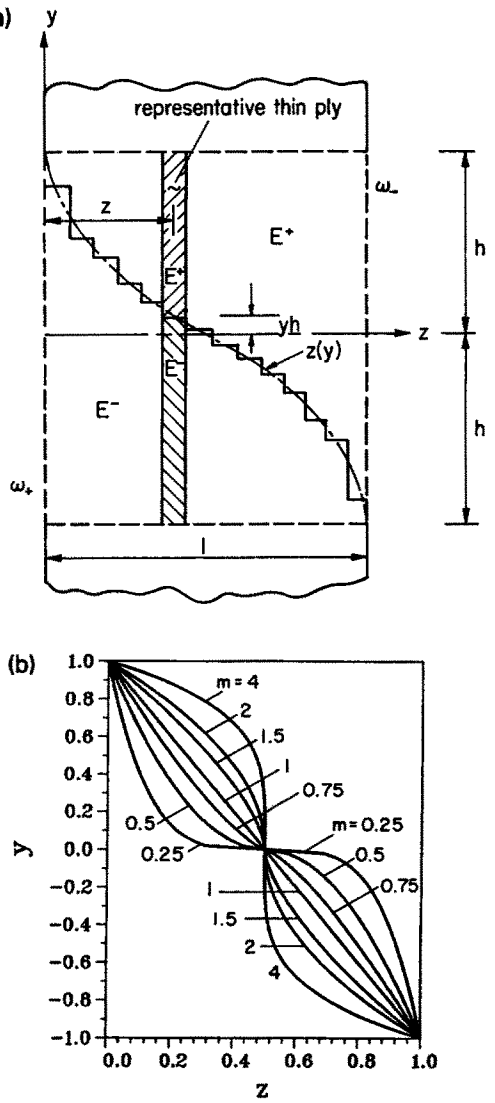

Fig. 4. Estimate of phase shifting angle, (a) multi-ply model, (b) a family of material transition function.

function in general can be any monotonically decreasing function satisfying the following boundary conditions of $z(1) = 0$ and $z(-1) = 1$.

We now apply formula (14) to each individual ply in the above multi-ply assembly. The remote compatibility of those thin plies are maintained by the common K^{∞} field, whereas the slight difference in the near tip fields between neighboring plies is neglected after averaging along the thickness. The linearity of $(K^{\text{tip}})^2$ with respect to the near tip modulus E^{tip} suggests the following approximation:

$$(K^{\text{tip}})^2 \approx -(K^{\infty})^2 \int_{-1}^{1} q(y)^2 \, e^{2i\omega(y)} \, (yh)^{2i\varepsilon} z'(y) \, dy. \tag{20}$$

Here K^{∞} is taken outside the integration because the remote bimaterial field is shared by all thin plies. The average $(K^{\text{tip}})^2$ on the left hand side of (20) could be phrased in terms of the right hand side of (14) squared. After dividing both sides in (20) by the common factor $(K^{\infty})^2$ and taking the phase angles of the remaining expressions, we arrive at the following estimate for the phase shift angle:

$$2\omega \approx \arg\left(-\frac{1+\alpha}{1-\alpha}e^{2i\omega_+}\int_{-1}^{0} y^{2i\varepsilon}z'(y)\,dy - e^{2i\omega_-}\int_{0}^{1} y^{2i\varepsilon}z'(y)\,dy\right), \tag{21}$$

where previously established relations (5), (15) and (16), as well as the step like property of $\omega(y)$ *and* $q(y)$ have been utilized in the above derivation. Equation (21) provides a general estimate for ω under any form of material transition functions, including the exponential function employed in the analysis of Delale and Erdogan (1988). It can be further simplified to:

$$2\omega \approx \arctan\left(\frac{\xi\sin 2\omega_+ + \sin 2\omega_-}{\xi\cos 2\omega_+ + \cos 2\omega_-}\right) + \arg\left(-\int_0^1 y^{2i\varepsilon}z'(y)\,dy\right), \quad \xi = \frac{1+\alpha}{1-\alpha}e^{-\pi\varepsilon}, \tag{22}$$

when $z'(y)$ is an even function of y. The first term in (22) represents an estimate for the phase shift angle for a transition layer having constant elastic moduli given by the mean of the neighboring bimaterial, while the second term characterizes the slope of material variation across the interlayer and has sign opposite to that for ε. The second term in (22) can be evaluated for specific form of the material transition function $z(y)$.

A typical family of $z(y)$ is:

$$z = (1-\operatorname{sgn}|y|^m)/2, \tag{23}$$

whose shapes for different values of the exponent m are plotted in Fig. 4(b). Substitution of (23) into (22) yields the following expression of ω:

$$2\omega \approx \arctan\left(\frac{\xi\sin 2\omega_+ + \sin 2\omega_-}{\xi\cos 2\omega_+ + \cos 2\omega_-}\right) - \arctan\frac{2\varepsilon}{m}. \tag{24}$$

The second term vanishes for large m because the material property in the transition layer becomes constant like. When m is small the second term becomes very large so that the interlayer model does not apply; in this case a redefinition of the interlayer thickness so as to give a finite m is appropriate. If the material property varies linearly across the inhomogeneous interface, $m = 1$ and the estimated values of ω for the range of α and β considered are listed in every first row of Table 1. The values of ω obtained by using the assumption in (18), namely:

$$\omega \approx 0.1584\alpha + 0.0630\beta - \tfrac{1}{2}\arctan\frac{2\varepsilon}{m}, \tag{25}$$

are listed in the second rows of Table 1. It can be seen that the approximation (25) agrees well with (24) for realistic range of α and β, and especially near the major diagonal of Table 1 where most bimaterial Dundur's parameters are clustered (Suga *et al.*, 1988).

It is helpful to distinguish the two different sources contributing to the phase shift: a contribution associated with the oscillation index ε, termed oscillation phase shift, and an intrinsic phase shift that does not depend on the stress oscillation. The latter shifts the near tip phase even in the absence of stress oscillation, i.e. the case of a real Hermitian matrix. Anticipating this classification, we split ω as:

$$\omega(\alpha,\beta) = \omega_0 + \varepsilon\ln\hat{\omega}, \quad \omega_0 = \omega(\alpha,0) \tag{26}$$

where the first and the second terms are intrinsic and oscillation phase shifts, respectively. The values of $\hat{\omega}$ are presented in Table 2. The physical significance of $\hat{\omega}$ will become transparent in the next section. The approximation anticipated in (25) leads to the following estimates of intrinsic and oscillation phase shifts:

Table 1. Phase shifting angles ω for isotropic bimaterials with a linear transition layer (every first and second row represents accurate and approximate values, respectively)

	α										
β	−0.8	−0.6	−0.4	−0.2	−0.1	0	0.1	0.2	0.4	0.6	0.8
−0.4	−0.2558	−0.2219	−0.1954	−0.1725	−0.1612	−0.1492	−0.1360	−0.1207	−0.0790	−0.0088	0.1287
	−0.2836	−0.2520	−0.2203	−0.1886	−0.1728	−0.1569	−0.1411	−0.1252	−0.0936	−0.0619	−0.030
−0.2	−0.2412	−0.1787	−0.1378	−0.1055	−0.0907	−0.0758	−0.0603	−0.0433	−0.0010	0.0627	0.1763
	−0.2035	−0.1718	−0.1401	−0.1085	−0.0926	−0.0768	−0.0609	−0.0451	−0.0134	0.0183	0.0499
−0.1	−0.2290	−0.1530	−0.1055	−0.0696	−0.0537	−0.0381	−0.0220	−0.0049	0.0360	0.0949	0.1965
	−0.1649	−0.1332	−0.1016	−0.0699	−0.0540	−0.0382	−0.0224	−0.0065	0.0252	0.0568	0.0885
−0.05	−0.2219	−0.1392	−0.0887	−0.0536	−0.0349	−0.0190	−0.0030	0.0140	0.0539	0.1101	0.2056
	−0.1458	−0.1141	−0.0824	−0.0508	−0.0349	−0.0191	−0.0032	0.0126	0.0443	0.0760	0.1076
−0.02	−0.2172	−0.1307	−0.0784	−0.0402	−0.0236	−0.0076	0.0085	0.0253	0.0645	0.1191	0.2108
	−0.1343	−0.1207	−0.0710	−0.0393	−0.0235	−0.0076	0.0082	0.0241	0.0557	0.0874	0.1191
0	−0.2141	−0.1249	−0.0715	−0.0327	−0.0161	0.0	0.0161	0.0327	0.0715	0.1249	0.2141
	−0.1267	−0.0950	−0.0634	−0.0317	−0.0158	0.0	0.0158	0.0317	0.0634	0.0950	0.1267
0.02	−0.2108	−0.1191	−0.0645	−0.0253	−0.0085	0.0076	0.0236	0.0402	0.0784	0.1307	0.2172
	−0.1191	−0.0874	−0.0557	−0.0241	−0.0082	0.0076	0.0235	0.0393	0.0710	0.1027	0.1343
0.05	−0.2056	−0.1101	−0.0539	−0.0140	0.0030	0.0190	0.0349	0.0536	0.0887	0.1392	0.2219
	−0.1076	−0.0760	−0.0443	−0.0126	0.0032	0.0191	0.0349	0.0508	0.0824	0.1141	0.1458
0.1	−0.1965	−0.0949	−0.0360	0.0049	0.0220	0.0381	0.0537	0.0696	0.1055	0.1530	0.2290
	−0.0885	−0.0568	−0.0252	0.0065	0.0224	0.0382	0.0540	0.0699	0.1016	0.1332	0.1649
0.2	−0.1763	−0.0627	0.0010	0.0433	0.0603	0.0758	0.0907	0.1055	0.1378	0.1787	0.2412
	−0.0499	−0.0183	0.0134	0.0451	0.0609	0.0768	0.0926	0.1085	0.1401	0.1718	0.2035
0.4	−0.1287	0.0088	0.0790	0.1207	0.1360	0.1492	0.1612	0.1725	0.1954	0.2219	0.2558
	0.0302	0.0619	0.0936	0.1252	0.1411	0.1569	0.1728	0.1886	0.2203	0.2520	0.2836

Table 2. Values of $\hat{\omega}$

	α										
β	−0.8	−0.6	−0.4	−0.2	−0.1	0.0	0.1	0.2	0.4	0.6	0.8
−0.4	0.1501	0.1928	**0.2349**	**0.2783**	**0.3026**	**0.3307**	**0.3647**	0.4087	0.5567	0.9369	2.5962
−0.2	0.0238	0.0627	0.1183	0.1949	**0.2453**	**0.3087**	**0.3930**	0.5115	0.9852	2.6437	15.369
−0.1	0.0008	0.0083	0.0368	0.1130	0.1863	**0.3037**	0.5017	0.8568	3.0851	19.497	470.0
−0.05	9×10^{-7}	0.00016	0.0038	0.0345	0.1119	**0.3031**	0.8306	2.4124	29.473	1×10^{3}	4×10^{5}
0.05	0.5870	**0.3951**	**0.3311**	**0.3093**	**0.3029**	**0.3031**	**0.3069**	**0.2693**	**0.3403**	0.4093	0.6142
0.1	0.5763	**0.3900**	**0.3288**	**0.3076**	**0.3033**	**0.3037**	**0.3082**	**0.3148**	**0.3452**	0.4157	0.6276
0.2	0.5568	**0.3814**	**0.3253**	**0.3080**	**0.3063**	**0.3087**	**0.3147**	**0.3237**	**0.3582**	0.4344	0.6571
0.4	0.5307	**0.3709**	**0.3276**	**0.3206**	**0.3237**	**0.3307**	**0.3409**	**0.3547**	**0.3991**	0.4871	0.7343

$$\omega_0 \approx 0.1584\alpha, \quad \hat{\omega} \approx 0.3. \tag{27}$$

The last number is representative of the magnitude of $\hat{\omega}$ in Table 2, where the $\hat{\omega}$ values ranging from 0.2 to 0.4 are marked by bold face typesets.

4. NEAR TIP CRACK MODE

The near tip crack mode is defined here as the phase angle ψ^{tip} of K^{tip}, where the latter is related to the near tip generalized traction. The expression of ψ^{tip} immediately follows from (14) and (12):

$$\psi^{\text{tip}} = \arg(K^{\infty}h^{i\varepsilon}) + \omega. \tag{28}$$

The physical significance of ω as a phase shifting angle is now evident. The structure of (28) pertains to aligned orthotropic bimaterials. Nevertheless as a first order approximation, the ω in (28) can be identified with the ω listed in Table 1, treated as functions of generalized Dundur parameters α and β defined in (5).

Insights on the near tip crack mode can be gained by considering detailed structure of the complex bimaterial stress intensity factor K^{∞}. To date, only one class of boundary value problems has been analyzed for generally anisotropic materials, namely a collinear array of cracks on the interface between two semi-infinite substrates. The stress intensity factors are found to be identical to their counterparts for isotropic bimaterials. For the example of the Griffith crack with crack length L, K^{∞} is:

$$K^{\infty} = t^{\infty}(1+2i\varepsilon)L^{-i\varepsilon}\sqrt{\pi L/2}, \tag{29}$$

where $t^{\infty} = \sigma_{22}^{\infty} + i\eta^{\infty}\sigma_{21}^{\infty}$ stands for applied remote traction to the Griffith crack and whose phase angle is denoted by ψ^{∞} in (10) (Suo, 1990). The value of ψ^{∞} would only depend on loading mode mixity for the special case of isotropic bimaterials.

Substituting (29) into (28), we obtain the following result on near tip crack mode of the Griffith crack:

$$\psi^{\text{tip}} = \psi^{\infty} + \arctan 2\varepsilon - \varepsilon \ln \frac{L}{h} + \omega, \tag{30}$$

where the last three terms contribute to what shall be referred to as the skewness of the interlayer problem. Substitution of the approximate relations (26) and (27) leads to the following explicit result:

$$\psi^{\text{tip}} = \psi^{\infty} + 0.1584\alpha - \varepsilon \ln \frac{L}{2.2h}. \tag{31}$$

At this juncture, it is appropriate to ask about the accuracy of the proposed multi-layer

Table 3. ψ^{tip} predictions compared with the Delale–Erdogan solution (1988)

a/h	Present solution	Delale–Erdogan ($\psi^{\infty} = 0$)	Delale–Erdogan ($\psi^{\infty} = \pi/2$)
1.0	4.446	5.124	5.076
2.0	6.264	6.989	7.020
4.0	8.082	8.269	8.304
8.0	9.901	8.998	8.990
10.0	10.486	9.178	9.182

model. The results of two independent evaluations are discussed below. First, the predictions of the multilayer model is compared with the analytical solution of Delale and Erdogan (1988) for a Griffith crack with crack length $L = 2a$. The bimaterial outside the interlayer of half-thickness h is characterized by elastic constants $E_+/E_- = 3$ and $\nu_+ = \nu_- = 0.3$, while the Young's modulus varies across the interlayer by:

$$E(x_2) = \sqrt{3}E_- e^{\beta_0 x_2/h}, \quad \beta_0 = \ln\sqrt{3}. \tag{32}$$

The near tip mode mixity is then given by (30) with ω calculated from (21). The latter can be written down more explicitly as:

$$2\omega \approx \arg\left\{\frac{1+\alpha}{1-\alpha} e^{2i\omega_+} \int_{-1}^{0} y^{2i\varepsilon} e^{\beta_0 y}\, dy + e^{2i\omega_-} \int_{0}^{1} y^{2i\varepsilon} e^{\beta_0 y}\, dy\right\}. \tag{33}$$

Listed in Table 3 are the $\psi^{tip} - \psi^{\infty}$ data (in degrees) calculated from (30) and (33) (under the assumption of $h \ll L$) and the analytical results of Delale and Erdogan (1988) for the two distinct cases of ψ^{∞} equals zero and $\pi/2$. It can be seen that the multi-layer estimate on the near tip mode mixity differs from the analytical solution by about 1°. For the interlayer geometry of $a/h = 10$, the q factor for the remote tension case takes the value of 1.060, quite close to the value of 1.064 determined by J-integral [see (13)], whereas the q factor for the remote shear case is 1.040, slightly less than the J-integral prediction.

We have also compared predictions by the multi-layer model with full-field numerical calculations for the boundary layer crack geometry, i.e. the geometry bounded by the outer circle depicted in Fig. 1. Tractions consistent with bimaterial K^{∞} field are prescribed along the outer circular boundary of radius R. The bimaterial elastic constants are taken as $E_+/E_- = 0.2$ and $\nu_+ = \nu_- = 0.3$. In the finite element model, the material properties across the interlayer vary according to the material transition function of (23), with m taken as 2. The q factor for this material prescription is then determined as 1.317. The crack configuration is discretized by a mesh consisting of 1488 quadrilateral elements which are focused at the crack tip. Further details of numerical calculation will be reported elsewhere (Guo *et al.*, 1992). The calculated fracture parameters for various relative interlayer thicknesses h/R are listed in Table 4. The results of $|K_{cal}^{tip}|$, the calculated magnitude of near tip stress intensity factor, and $\psi_{cal}^{tip} - \psi^{\infty}$, the calculated near tip mode mixity shift, are the

Table 4. Boundary layer calculations on near tip fracture parameters

h/R	$\lvert K_{cal}^{tip}\rvert/\lvert K^{tip}\rvert$	ψ_{cal}^{tip}	ψ^{tip}
0.01	0.985	18.759	19.380
0.02	0.974	21.096	21.817
0.03	0.966	22.573	23.243
0.04	0.956	23.511	24.255
0.05	0.951	24.198	25.040
0.06	0.945	24.746	25.681
0.08	0.934	25.502	26.693
0.10	0.924	26.208	27.478
0.15	0.902	27.469	28.903
0.20	0.884	28.415	29.915

mean values of two calculations for ψ^∞ equal to zero and $\pi/4$, respectively. $|K_{\text{cal}}^{\text{tip}}|$ is normalized by $|K^{\text{tip}}|$ the value given by the J-integral prediction. It can be seen that the J-integral prediction is accurate to within 5% provided the relative thickness of interlayer is less than 0.05. The multi-layer estimate of $\psi^{\text{tip}}-\psi^\infty$ [evaluated from (30) and (24)] is listed in the last column in Table 4. The good agreement with the finite element result for mode mixity shift can be seen. It may also be observed that the agreement becomes better as the relative interlayer thickness h/R becomes small, justifying the present phase shift estimate.

In the literature on interfacial fracture, a frequently quoted definition of the near tip mode is:

$$\hat{\psi} = \arg\{t(\hat{L})\}, \tag{34}$$

where t is the complex generalized traction defined previously. The angle $\hat{\psi}$ is termed local mode mixity when the interfaces are treated as a mathematically sharp surface, e.g. Rice (1988), Rice *et al.* (1990), Suo (1990), Wang *et al.* (1992). The local mode mixity angle in (34) is defined relative to a length parameter $\hat{L}$ which can be chosen arbitrarily. Within the present model, this length parameter can be precisely fixed at:

$$\hat{L} = \hat{\omega}h \approx 0.3h. \tag{35}$$

This provides an interpretation of $\hat{\omega}$ tabulated in Table 2 as the dimensionless location where the mode mixity can be assessed from the results provided by conventional bimaterial analysis. If the near tip mode mixity $\hat{\psi}$ is previously determined by a length scale $\hat{L}$ other than the one given by (35), the actual crack tip mode can be recovered using the following translation law:

$$\psi^{\text{tip}} = \hat{\psi} - \varepsilon \ln(\hat{L}/\hat{\omega}h). \tag{36}$$

We next examine the condition under which the crack tip will be open. The present model predicts a truly open crack, free of any stress oscillation and Comninou type near tip contact zone (Comninou, 1977), as long as $|\psi^{\text{tip}}|$ evaluated by (30) is less than $\pi/2$. Thus, the crack will be genuinely open if the load angle ψ^∞ falls within the range of $\psi_+ \geqslant \psi^\infty \geqslant \psi_+ - \pi$. The upper limit ψ_+ for an open crack is:

$$\psi_+ = \pi/2 - \omega_0 - \arctan 2\varepsilon + \varepsilon \ln \frac{L}{\hat{\omega}h}, \tag{37}$$

and $\psi_+ - \pi/2 - \omega_0$ is almost symmetric with respect to the sign change of ε. Alternatively, an open crack is formed if:

$$\exp[-(\pi/2 - \psi^\infty - \omega_0)/\varepsilon] < c_{\text{open}} \frac{h}{L} < \exp[(\pi/2 + \psi^\infty + \omega_0)/\varepsilon], \tag{38}$$

where the dimensionless coefficient $c_{\text{open}} = 7.389\hat{\omega} \approx 2.2$. The resemblance of this "openness" condition with the nonoscillatory condition (9) is emphasized here and difference between c_{oscil} and c_{open} is not substantial, say less than one order of magnitude. The concept of a small scale contact zone introduced by Rice (1988) to circumvent the issue of interpenetration can be justified because no contact would ever exist if $\psi_+ \geqslant \psi^\infty \geqslant \psi_+ - \pi$. Indeed the related problems of stress oscillation and near tip contact can be removed simultaneously via the interlayer model under the common range of remote loading phase angle restricted by (9) and (38). Consequently, nonoscillatory and open crack tip profile will be realized for the range of realistic bimaterial descriptions if the present interlayer model is adopted, and the corresponding remote loading phase range would have an angle span slightly less than 180°, as suggested by Shih and Asaro (1989).

The in-plane mixed mode fracture condition within the interlayer is now stated by an intrinsic fracture curve Γ phrased in terms of the crack tip phase angle ψ^{tip}:

$$\mathcal{G}(\psi^{tip}) = \Gamma(\psi^{tip}), \tag{39}$$

where $\Gamma(\psi^{tip})$ could be obtained by a micromechanical model of the interlayer. The Γ curve defined in (39) represents intrinsic fracture resistance and its shape is unaffected by the oscillation index ε, as suggested by Hutchinson (1990). The values of ε, as well as the specimen geometry (through dimensionless length L/h), only contribute to the shifting of this intrinsic curve via ψ^{tip}.

Various experimentally determined interface fracture resistance curves can be reorganized and compiled in a unified and unambiguous manner using formula (36). The commonly observed U-shape curve of interface toughness vs mode mixity is preserved but the toughness is a minimum near $\psi^{tip} = 0$. For example, the experimentally measured interface toughness curve reported by Liechti and Chai (1992) can be made approximately symmetric by a phase shift of about 20–25°. For their glass/epoxy bimaterial and test configuration, a phase shift of 25° would require an interface thickness of the order of 10 microns. A width of this order is resonable because the glass/epoxy interface is rather diffused.

5. FRACTURE CHARACTERIZATION FOR A PARTIALLY "CLOSED" CRACK

We next discuss the case of a partially closed interlayer crack in which the major portion of the crack length ($R < -x_1 < L$) is open but the crack tip is closed by the skewness of the near tip field, as shown in Fig. 5(a). A mathematical description for this situation is

$$\mathrm{Re}\,[e^{i\omega} K^{\infty} h^{i\varepsilon}] < 0 \quad \text{but} \quad \mathrm{Re}\,[K^{\infty} L^{i\varepsilon}] > 0. \tag{40}$$

The other cases involving totally closed interlayer cracks under the condition $\mathrm{Re}\,[K^{\infty} L^{i\varepsilon}] < 0$ are of less interest. A contact traction $t_c = \sigma_c + i\eta\tau_c$ would occur along $-R < x_1 < 0$, with real normal contact stress σ_c and friction stress τ_c. For simplicity, attention is focused on the case of frictionless contact in which $t_c = \sigma_c \geqslant 0$. The near tip stress singularity field can be constructed by the superposition of a non-contact problem with hypothetical material overlapping, see Fig. 5(b), and a stress field solely generated by the normal contact stress, i.e.

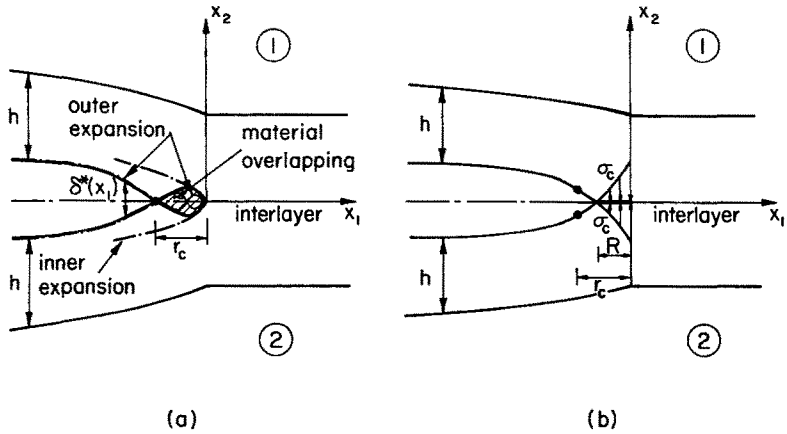

Fig. 5. Geometry of crack tip contact, (a) contact configuration, (b) hypothetical crack profile after the release of contact stress.

$$K^{\text{tip}} = q\,e^{i\omega}K^{\infty}h^{i\varepsilon} + K^{c} = iK_{\text{II}}^{\text{tip}}, \tag{41}$$

where $K_{\text{II}}^{\text{tip}}$ is real and the near tip phase angle is fixed at $\pm 90°$. A simple estimate for the stress intensity factor K^c induced by contact traction σ_c can be made by a suitable application of the following formula of Suo (1990):

$$K^{c} \approx -\sqrt{\frac{2}{\pi}}\cosh \pi\hat{\varepsilon} \int_{-R}^{0} (-x_1)^{-1/2-i\hat{\varepsilon}}\sigma_c(x_1)\,dx_1, \tag{42}$$

for bimaterial with oscillation index $\hat{\varepsilon}$. Equation (42) can be used for the present interlayer model if the value of $\hat{\varepsilon}$ varies gradually from zero (when $|x_1| \ll h$) to ε (when $|x_1| \gg h$).

We next describe a scenario of crack tip contact. In the absence of contact traction, the crack face opening displacement $\delta^*(x_1)$, for aligned orthotropic materials, should have the following asymptotic form:

$$\delta^*(x_1) = \begin{cases} \sqrt{-2x_1/\pi}H_{22}^{\text{tip}}\,\text{Re}\,[q\,e^{i\omega}K^{\infty}h^{i\varepsilon}], & \text{if } |x_1| \ll h; \\ \sqrt{-2x_1/\pi}(H_{22}^{\infty}/\cosh \pi\varepsilon)\,\text{Re}\,[K^{\infty}(-x_1)^{i\varepsilon}/(1+2i\varepsilon)], & \text{if } |x_1| \gg h, \end{cases} \tag{43}$$

as shown in Fig. 5(b). Note by condition (40), the last factors of the respective two asymptotic expressions possess different signs. The sign switch of δ^* occurs at a location which could be represented fairly well by the first contact distance r_c estimated from the outer field, Rice (1988). The application of contact traction σ_c eliminates the material overlapping shown in the shaded area of Fig. 5(b), and the contact zone size R would be a finite fraction of r_c. The case of $R \ll h$ is termed here as the case of small scale interlayer contact, and it should not be confused with the concept of small scale contact which requires R to be small with respect to the radius of K^{∞} dominant annulus. In this case one can take $\hat{\varepsilon} = 0$ and consequently the values of K^c (now becomes real) and $K_{\text{II}}^{\text{tip}}$ are directly evaluated from the remote K^{∞}:

$$K^{c} = -\text{Re}\,[q\,e^{i\omega}K^{\infty}h^{i\varepsilon}], \quad K_{\text{II}}^{\text{tip}} = \text{Im}\,[q\,e^{i\omega}K^{\infty}h^{i\varepsilon}]. \tag{44}$$

The case of large scale interlayer contact (referring $R \gg h$) is more involved. The well-known Comninou solution (1977) (which introduces frictionless contact to eliminate mutual penetration near the tip of an interface crack) would provide an accurate outer field for the present interlayer fracture problem. The normal contact stress in the Comninou solution, however, is unbounded near the crack tip, and then drops to a bounded normal stress immediately behind the crack tip. This rather peculiar behavior can be eliminated by the present interlayer model. The boundedness of σ_c in the context of small and intermediate scale interlayer contact is demonstrated below. The same qualitative behavior would be preserved in the case of large scale interlayer contact.

We first phrase the nonoverlapping condition along the contact region as:

$$\frac{H_{22}^{\text{tip}}}{\pi\sqrt{-x_1}}\int_{-R}^{0}\frac{\sqrt{-s}}{s-x_1}\sigma_c(s)\,ds = -\frac{d\delta^*}{dx_1} \quad \forall\, x_1 \in (-R, 0), \tag{45}$$

where the left hand side represents the x-derivative of interlayer crack opening displacement for orthotropic materials, derivable from the result reported by Suo (1990). If the function δ^* is known, we can appeal to the following singular integral equation of Cauchy type for the contact stress σ_c,

$$\frac{1}{\pi}\int_{-1}^{1}\frac{\sqrt{1+t}}{t-x}\sigma_c(t)\,dt=\frac{K^c}{\sqrt{\pi R}}f(x),\quad x_1=-R(1+x)/2, \tag{46}$$

where

$$f(x)=\delta(x)+2(1+x)\delta'(x),\quad \delta^*(x_1)=-K^cH_{22}^{tip}\sqrt{\frac{-2x_1}{\pi}}\,\delta(x). \tag{47}$$

Therefore $f(x)$ is a bounded positive function and decreases monotonically from $f(-1)=1$, according to eqn (43) and the situation presented in Fig. 5(b). Consider $y(x)=\sqrt{1+x\sigma_c(x)}$ as the unknown function to be resolved under the prescription of $f(x)$. Equation (46) then stands for a canonical Cauchy integral equation for $y(x)$. For the present "soft contact" situation (Erdogan, 1978), the solution of $y(x)$ should be bounded at both ends of $x=\pm 1$. That requirement would be sufficient to give the following expression for σ_c,

$$\sigma_c=\frac{K^c}{\sqrt{\pi R}}\frac{\sqrt{1-x}}{\pi}\int_{-1}^{1}\frac{f(t)\,dt}{(x-t)\sqrt{1-t^2}}. \tag{48}$$

The normal contact stress estimated by the interlayer fracture model has the appealing feature of being finite at the crack tip and diminishing at the contact edge, as conjectured in Fig. 5(b). Moreover, the strength of contact stress is measured by $K^c/\sqrt{\pi R}$ where K^c is given by (44). In contrast, the Comninou model of interface fracture (1977) predicts singular contact normal stresses with amplitude related to the local K_{II} by a ratio of β, the second of Dundur's parameter.

A fracture criterion for partially closed interlayer crack could be phrased in terms of a critical near tip shear stress intensity factor, K_{II}^{tip}, which is defined in (41) and resolved explicitly in (44) for the case of small scale interlayer contact. Alternatively, failure could also be induced by the coalescence of microcracks within the interlayer onto the main crack. The microcracks are initiated at some distance ahead of the main crack where the tensile hoop stress σ_{22} is high, as schematically shown in Fig. 5(a). The competition between near tip shearing versus remote tensile cracking provides the mechanism dominating the interlayer fracture.

6. DISLOCATION EMISSION FROM AN INTERLAYER CRACK TIP

The plasticity aspects of interface cracks have been reviewed by Shih (1991). He has observed that the domain of validity of a separable asymptotic solution, if one exists, of a stationary interface crack is smaller than length scales of physical relevance. Through full-field calculations for a Griffith crack lying at the interface between an elastic-plastic material and a rigid substrate, Sharma and Aravas (1992) have shown that the region dominated by the separable asymptotic solutions obtained by Wang (1990) and Champion and Atkinson (1991) is very small indeed. Thus it does not appear that a continuum plasticity treatment can provide the relevant results to extend the present interlayer fracture framework. Moreover, the validity of continuum plasticity theory is questionable at length scales pertinent to interlayer thickness. Therefore, we explore an alternative approach based on discrete dislocations to study ductile/brittle interlayer fracture behavior.

To gain some understanding of interlayer ductile fracture we analyze the geometry shown in Fig. 6. This treatment is as an extension of Rice–Thomson model (1974) for homogeneous materials. We investigate the competition between dislocation emission (with consequential crack tip blunting) and interlayer cleavage by considering the onset of dislocations originally situated at (ρ,ϕ), where ρ is the feasible distance for dislocation nucleation and ϕ the angle between glide plane and interface. Direct evidence confirming this geometry has been recently reported by Zhang and Thomson (1990). Their micrographs

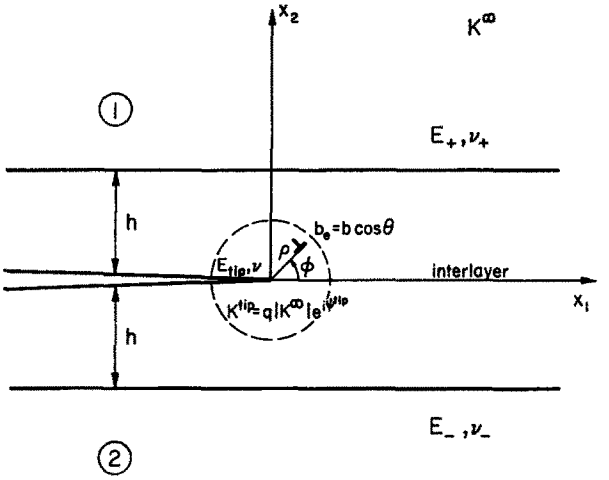

Fig. 6. Dislocation emission from a crack tip advancing in an interlayer, described by Rice–Thomson dislocation emission mechanism.

showed arrays of dislocations, of similar orientations, were emitted at regular intervals from the tip of an advancing interface crack.

By analysis parallel to that which was given by Rice and Thomson (1974), a one-to-one correspondence between the dislocation emission angle ϕ and the near tip mode mixity ψ^{tip} is obtained:

$$\frac{2\cos\phi - \tan(\phi/2)\sin\phi}{\tan(\phi/2)(3\cos\phi - 1) + 6\sin\phi} = \tan\psi^{tip}, \tag{49}$$

by neglecting the ledge force term. The dislocation emission angle versus near tip mode mixity is shown by the solid curve in Fig. 7. ϕ decreases monotonically as ψ^{tip} increases and ϕ changes rapidly near $\phi = 0$.

The condition for dislocation emission can be stated in the following form:

$$\rho = \hat{\rho}/R_m^2 \leqslant \rho_c, \tag{50}$$

where ρ_c represents the feasible nucleation site of dislocation and has a value larger than r_0 (the dislocation core cutoff radius) if energy fluctuation and three dimensional effect are taken into account. $\hat{\rho}$ in (50) corresponds to the case of purely mode I near tip field:

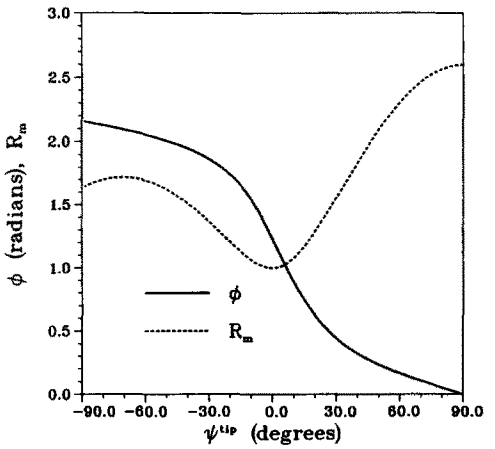

Fig. 7. Effect of crack tip mode mixity on dislocation emission parameters. Solid and dashed curves correspond to emission angle ϕ and driving intensity R_m, respectively.

$$\hat{\rho} = \frac{E^{\text{tip}} b^2}{16\pi\gamma R_0^2}\left(\frac{1-\nu\sin^2\theta}{\cos\theta}\right)^2, \tag{51}$$

where $R_0 = 0.7698$ denotes the maximum value of $\sin\phi\cos(\phi/2)$, b refers to the magnitude of the Burgers vector, θ is the angle between the Burgers vector and the dislocation line, and γ signifies the true/actual surface energy along the interlayer. The numerical factor R_m in (50) characterizes the enhancement of dislocation driving force by near tip mode mixity. It is given by:

$$R_m = \cos(\phi/2)[\sin\phi\cos\psi^{\text{tip}} + (3\cos\phi - 1)\sin\psi^{\text{tip}}]/R_0 \tag{52}$$

with ϕ determined by (49). The relation between R_m and ψ^{tip} indicated by the dashed curve in Fig. 7 shows the influence of crack tip mode mixity on the dislocation driving intensity. The minimum value of R_m is obtained under pure mode I near tip field and R_m reaches its maximum when the near tip field is purely mode II. Consequently, dislocation emission is assisted by the mixed mode conditions induced by the skewness of the interlayer fracture.

7. CONCLUDING REMARKS

Clarifications of several intriguing issues in interfacial fracture are achieved via a physically motivated interlayer model. The mathematical structure for the interlayer model is easily identified by an application of the J integral. Only the phase shift angle, which is essential in formulating concepts of near tip skewness and near tip contact, remains to be worked out. For aligned orthotropic materials, explicit results for the phase shift have been obtained for a class of material transition function. The framework which incorporates a length dimension of an interlayer provides precise definitions of local mode mixity, "open crack" and intrinsic fracture toughness curve, and unifies several concepts and aspects of interfacial fracture. Within this framework, stress oscillation and singularity in contact stresses (caused by a mathematically sharp interface) are not issues at all.

The interlayer model developed here can be extended into the case of dynamic crack growth. This problem has been recently examined by Yang *et al.* (1991) who showed that the oscillation index ε becomes exceedingly large when crack speed approaches the lower Rayleigh wave speed. These results pertaining to a mathematically sharp interface can be reinterpreted in the light of interlayer fracture concepts.

Acknowledgements—Wei Yang and C. Fong Shih are supported by the Office of Naval Research through ONR Grant N00014-90-J1380. The computations were carried out at the Computational Mechanics Research Facility within the Division of Engineering of Brown University. This work and an earlier version of the manuscript was completed during Wei Yang's visit to Brown University from July to October, 1990. The visit of Wei Yang to Brown University was partially supported by the Fok Ying Tung Education Foundation.

REFERENCES

Ahn, V. S., Achenbach, J. D., Li, Z. L. and Kim, J. O. (1991). Numerical modelling of the $V(z)$ curve for a thin-layer/substrate configuration. *Research in Nondestructive Evaluation* (in press).

Comninou, M. (1977). The interface crack. *J. Appl. Mech.* **44**, 631–636.

Champion, C. R. and Atkinson, C. (1991). A crack at the interface between two power-law materials under plane strain loading. *Proc. Royal Society, London* **A432**, 547–553.

Delale, F. and Erdogan, F. (1988). On the mechanical modelling of the interfacial region in bonded half-planes. *J. Appl. Mech.* **55**, 317–324.

Erdogan, F. (1978). Mixed boundary-value problems in mechanics. In *Mechanics Today* (Edited by S. Nemat-Nasser) **4**, 1–86.

Guo, Z. T., Cheng, L. and Yang, W. (1992). Numerical modelling of interlayer fracture (in press).

Hutchinson, J. W., Mear, M. E. and Rice, J. R. (1987). Crack paralleling an interface between dissimilar materials. *J. Appl. Mech.* **54**, 828–832.

Hutchinson, J. W. (1990). Mixed mode fracture mechanics of interfaces. In *Metal-Ceramic Interfaces, Acta-Scripta Metallurgica Proc. Series 4*, Pergamon Press, New York, 295–306.

Hutchinson, J. W. and Suo, Z. (1992). Mixed mode cracking in layered materials. *Advances in Applied Mechanics*, Vol. 29, pp. 63–191. Academic Press, New York.

Liechti, K. M. and Chai, Y-S. (1992). Asymmetric shielding in interfacial fracture under in-plane shear. *J. Appl. Mech.* **59**, 295–304.

Nix, W. D. (1989). Mechanical properties of thin films. *Metall. Trans.* **20A,** 2217–2245.
O'Dowd, N. P., Stout, M. G. and Shih, C. F. (1992). Fracture toughness of alumina-niobium interfaces: experiments and analyses. *Philosophical Magazine* **A66,** 1037–1064.
Rice, J. R. (1988). Elastic fracture mechanics concepts for interfacial cracks. *J. Appl. Mech.* **55,** 98–103.
Rice, J. R., Suo, Z. and Wang, J. S. (1990). Mechanics and thermodynamics of brittle interfacial failure in bimaterial systems. In *Metal-Ceramic Interfaces, Acta-Scripta Metallurgica Proc. Series 4*, Pergamon Press, New York, 269–294.
Rice, J. R. and Thomson, R. (1974). Ductile versus brittle behavior of crystals. *Philosophical Magazine* **29,** 73–97.
Ruhle, M., Evans, A. G., Ashby, M. F. and Hirth, J. P. (eds) (1990). *Metal-Ceramic Interfaces, Acta-Scripta Metallurgica Proc. Series 4*, Pergamon Press, New York.
Sharma, S. M. and Aravas, N. (1992). On the development of variable-separable asymptotic elastoplastic solutions for interface cracks (in press).
Shih, C. F. and Asaro, R. J. (1988). Elastic-plastic analysis of cracks on bimaterial interfaces: part I—small scale yielding. *J. Appl. Mech.* **55,** 299–316.
Shih, C. F. and Asaro, R. J. (1989). Elastic-plastic analysis of cracks on bimaterial interfaces: part II—structure of small scale yielding field. *J. Appl. Mech.* **56,** 736–799.
Shih, C. F. (1991). Cracks on bimaterial interfaces: elasticity and plasticity aspects. *Mater. Sci. Engng* **A143,** 77–90.
Suga, T., Elssner, E. and Schmander, S. (1988). Composite parameters and mechanical compatibility of material joints. *J. Composite Mater.* **22,** 917–934.
Suo, Z. (1990). Singularities, interfaces and cracks in dissimilar anisotropic media. *Proc. Royal Society, London* **A427,** 331–358.
Suo, Z. and Hutchinson, J. W. (1989). Sandwich test specimens for measuring interface crack toughness. *Mater. Sci. Engng* **A107,** 135–143.
Wang, T. C. (1990). Elastic-plastic asymptotic fields for crack on bimaterial interfaces. *Engng Frac. Mech.* **37,** 527–538.
Wang, T. C., Shih, C. F. and Suo, Z. (1992). Mechanics of interface crack extension and kinking in anisotropic solids. *Int. J. Solids Struct.* **29,** 327–344.
Whan, R. E. (ed.) (1986). *Metals Handbook*, Ninth Edition, Vol. 10, Materials Characterization, American Society of Metals, Metals Park, Ohio.
Yang, W., Suo, Z. and Shih, C. F. (1991). Mechanics dynamic debonding. *Proc. of the Royal Society, London* **A433,** 679–697.
Zhang, H. and Thomson, R. (1990). Private communications.